A novel combined model of discrete and mixture phases for nanoparticles in convective turbulent flow

Mostafa Mahdavi, Mohsen Sharifpur* and Josua P. Meyer

*Corresponding author

*Tel: +27 12 420 2448 *Email: mohsen.sharifpur@up.ac.za

Department of Mechanical and Aeronautical Engineering, University of Pretoria,

Private Bag X20, Hatfield, 0028, Pretoria, South Africa.

Abstract

In this study, a new combined model presented to study the flow and discrete phase features of nano-size particles for turbulent convection in a horizontal tube. Due to the complexity and also many phenomena involved in particle-liquid turbulent flows, the conventional models are not able to properly predict some hidden aspects of the flow. Therefore, Brownian motion is implemented in discrete phase model to predict the migration of the particles as well as energy equation has modified for particles. Then, the final results are exported to the mixture equations of the flow. The effects of the mass diffusion due to thermophoresis, Brownian motion and turbulent dispersion are implemented as source terms in equations. The results are compared with the experimental measurements from literature and are adequately validated. The accuracy of predicted heat transfer and friction coefficients are also discussed versus measurements. The migration of the particles toward the centre of the tube is properly captured. The results show the non-uniform distribution of particles in turbulent flow due to strong turbulent dispersion. The proposed combined model can open new viewpoints of particle-fluid interaction flows.

Keyword: discrete phase, turbulent flow, nanoparticles, turbulent dispersion, diffusion terms

1 Introduction

The main advantage of mixing ultrafine particles with a fluid is concerned to the enhancement of heat transfer in convective flows. This can happen only in certain circumstances depending on the type of the flow and particles. Therefore, modelling and numerical methods can be appropriate tools for predictions of heat transfer and pressure loss when there is no experimental data.

Improvement and deterioration in heat transfer by particle-fluid flows were both reported by researchers in forced convection flows for different geometries. For instance, in the laminar and turbulent flow of heat exchangers [1–5], horizontal and vertical tubes [6–14], microchannel [15–17], etc. Bajestan et al. [1] considered the Brownian motion as the dominant mechanism of heat transfer in laminar flow. He et al. [10] and Sonawane et al. [3] presented Brownian motion as the reason of non-uniform distribution of particles. This approach could result the non-uniform scattering of viscosity and thermal conductivity in the main flow. Liu and Yu [17], Utomo et al. [7] and Xuan and Li [14] reported the Brownian motion and thermophoresis diffusion are the main contributing factors in the enhancement of heat transfer, rather than thermal conductivity improvement. Although, the effects of Brownian motion and thermophoresis parameters were considered minor by Ahmad [18].

Regarding numerical modelling, mixture model has been used in recent years as the simplest method. A small slip velocity between nanoparticles and fluid is assumed in this model, and the only effective parameters are concerned to transport properties. Avramenko et al. [19], Öğüt and Kahveci [20], Safikhan and Abbassi [21] and Selvakumar and Dhinakaran [22] are the examples of using mixture

model. The modelling results were found in good agreement with experiments for heat transfer and pressure drops. Nonetheless, they did not predict the relative velocity because of using the default and simple algebraic model. Consequently, particles were shown uniformly distributed in the domain. It means that the capabilities of mixture model regarding these cases can be still in doubt. This model was somehow developed by Buongiorno [23] via considering mass diffusion effects of nanoparticles due to concentration and temperature gradient. He stated that turbulent diffusion should be dominant rather than Brownian diffusion in the matter of turbulent flow. Avramenko et al. [24] mentioned the weak impacts of nanoparticles on transport processes in a turbulent boundary layer compared to laminar flows. Other approaches were also developed by Mahdavi et al. [25,26] by proposing new slip velocity and diffusion terms in mixture governing equations.

The other new approach of nanofluid simulations is known as Discrete Phase Modelling (DPM) which has only been used in very recent years. The interaction forces and heat transfer can exchange between particles and liquid in DPM. Since particles are individually tracked in the Lagrangian frame, the number of particles plays an important role in the final solution. Kumar and Puranik [27], Mahdavi et al. [28,29], Rashidi et al. [30] and Shirvan et al. [31] employed discrete model for nano-size particles in different flows. They considered drag, lift, Brownian, virtual mass, pressure gradient and thermophoretic forces acting on a single particle. The default model from a CFD software was used in the simulations with no modified equations. Since the phenomena in nanoscale are totally different than micro-scale, for example, the electrostatic adhesive and repulsive forces are important in particle-particle and particle-wall in contact. This is not considered in the DPM and further developments are required for this case as well as cluster formation.

The main approaches in nanofluid simulations were presented in this section as a mixture and discrete phase. The literature review showed that most of the numerical modellings were conducted via these methods and only some of them were referred in this section as examples. It can also be concluded that both models considered some essential aspects of simulations, but not the entire. In this study, a novel method is used to combine those above-mentioned approaches for particle-fluid flow. Alumina and zirconia nanofluids are chosen as heat transfer fluids in turbulent convective flow in a tube. The implemented equations are critically explained and the numerical procedure is subsequently described.

2 Mathematical description of equations and implementation

2.1 Physics of the Problem

The developed model in this report is compared to experimental measurements from Williams et al. [32]. Aluminium oxide and zirconium oxide particles are used as: aluminium oxide with 46 nm size, density 3920 kg/m^3, specific heat 880 J/kg.K and thermal conductivity 35 W/m.K, and zirconium oxide with 60 nm size, density 5500 kg/m^3, specific heat 502 J/kg.K and thermal conductivity 2 W/m.K. They are mixed with distilled water with different volume fraction of 0.009 to 0.036 for alumina and 0.002 to 0.005 for zirconia. The flow is turbulent in a horizontal tube of inner diameter 0.0094 m and nearly 3 m in length. Uniform heat flux is applied on the outer surface of the tube. It is noted that the gravity and buoyancy force are present in both particles and fluid flow to ensure capturing the possibility of secondary flow.

2.2 Discrete phase modelling

A representative particle in each computational cell is solved in the Lagrangian frame and extended to other particles. The force balance equation of motion for particles is as follows:

$$m_p \frac{d\vec{u}_p}{dt_p} = F_{drag} + m_p \frac{\vec{g}(\rho_p - \rho_c)}{\rho_p} + F_{lift} + F_{virtual} + F_{magnus} + F_{thermo} + F_b + F_{pressure} \quad (1)$$

The interaction forces in particle motion equation are briefly explained here:

Drag force [33], which is valid for any ranges of Reynolds number:

$$F_{drag} = \frac{m_p}{\tau} \frac{C_D Re_p}{24 C_c} \left(u_c - u_p\right) \quad (2)$$

$$Re_p = \frac{\rho_c d_p \left|u_c - u_p\right|}{\mu_c} \quad (3)$$

Lift force [34]:

$$F_{lift} = 20.3 \mu_c d_p^2 (u_c - u_p) \sqrt{\frac{\dot{\gamma}\rho_c}{\mu_c}} \operatorname{sgn}(\dot{\gamma}) \quad (4)$$

where $\dot{\gamma}$ is the shear rate mainly important at the vicinity of the walls. The other form of lift force can be found in Saffman [35]. However, this correlation can be used for particles smaller than micro-size.

Pressure gradient and virtual mass forces [36]:

$$F_{pressure} = m_p \left(\frac{\rho_c}{\rho_p}\right) u_p \nabla u_c \quad (5)$$

$$F_{virtual} = 0.5 m_p \left(\frac{\rho_c}{\rho_p}\right) \frac{d}{dt}(u_c - u_p) \quad (6)$$

Magnus force: the particle angular velocity, ω_p, can be obtained from particle conservation of angular momentum equation [37,38]:

$$I_p \frac{d\omega_p}{dt} = \frac{\rho_c}{2} \left(\frac{d_p}{2}\right)^5 C_\omega \Omega \quad (7)$$

$$\Omega = \frac{1}{2} \nabla \times u_c - \omega_p \quad (8)$$

$$I_p = \frac{\pi}{60}\rho_p d_p^5 \tag{9}$$

$$C_\omega = \frac{6.45}{\sqrt{Re_{\omega_p}}} + \frac{32.1}{Re_{\omega_p}} \tag{10}$$

$$Re_{\omega_p} = \frac{\rho_c |\Omega| d_p^2}{4\mu_c} \tag{11}$$

The general form of Magnus lift force can be written as:

$$F_{Magnus} = \frac{1}{2} A_p C_{ML} \rho_c \frac{|u_c - u_p|}{|\Omega|}\left[\left(u_c - u_p\right)\times\Omega\right] \tag{12}$$

$$C_{ML} = 0.45 + \left(\frac{Re_{\omega_p}}{Re_p} - 0.45\right) exp\left(-0.05684 Re_{\omega_p}^{0.4} Re_p^{0.3}\right) \tag{13}$$

where A_p and C_{ML} are projected particle surface area and rotational lift coefficient respectively. This correlation is valid for $Re_p < 2000$.

Thermophoretic force [39]:

$$F_{thermo} = -C_T \frac{\nabla T}{T} \tag{14}$$

$$C_T = 0.78 \frac{\pi \mu_c^2 d_p}{\rho_c} \frac{k_c}{2k_c + k_p} \tag{15}$$

Brownian motion force. The default form of Brownian force is as follows [40]:

$$F_b = \zeta_i \sqrt{\frac{6\pi d_p \mu_c K_B T}{\Delta t_p}} \tag{16}$$

where ζ_i is the unit variance random number produced by a Gaussian white noise process.

The following equation is chosen and implemented for Gaussian white noise function [41,42]:

$$\zeta_1 = \sqrt{-2\ln U_1}\cos(2\pi U_2) \tag{17}$$

$$\zeta_2 = \sqrt{-2\ln U_1}\sin(2\pi U_2) \tag{18}$$

where U_i are uniform random numbers defined in the program. The final form of the code produces the random values in each direction. For random values $U<0.5$, ζ_1 is applied in Brownian force, and else ζ_2.

2.3 Heat transfer equation

Conservation of energy for a particle can be expressed and implemented as follows [43]:

$$m_p C_{p_p} \frac{dT_p}{dt} = m_c C_{p_c} \frac{DT_c}{Dt} - 2\pi d_p k_c (T_p - T_c) \tag{19}$$

where m_c is the mass of the fluid occupying the particle place. The first term on the right-hand side (material derivative) is the variation of internal energy of the fluid being in the place of the particle. This term is similar to the virtual mass term in force balance equation of the particles. The second term is obviously due to heat conduction from the surface of the nanoparticle. The solution of this ODE will be:

$$T_p^{t+\Delta t} = c_3 + \left[T_p^t - c_3\right] e^{-c_4 \Delta t} \tag{20}$$

$$c_3 = \frac{m_c C_{p_c}}{2\pi d_p k_c}\frac{DT_c}{Dt} + T_c \tag{21}$$

$$c_4 = \frac{m_c C_{p_c}}{2\pi d_p k_c} \tag{22}$$

2.4 Particles migration due to turbulent eddies

The effects of fluctuating velocity on particles trajectory are modelled using discrete random walk model developed by Bayazit [44]. The random fluctuating value of velocity during eddy lifetime is defined as:

$$u_i' = \xi\sqrt{\overline{u_i'^2}} \tag{23}$$

where ξ is the randomly distributed number from Gaussian pdf and $\sqrt{\overline{u_i'^2}} = \sqrt{\frac{2}{3}\kappa}$ is the root mean square of fluctuating velocity, with κ as the turbulent kinetic energy. This fluctuating velocity is considered in particle motion equation as $u_i = \overline{u}_i + u_i'$ and the subscript i refers to an individual velocity component. The interaction between the eddy and the particle occurs during the minimum of two characteristic times, the lifetime of the eddy and particle eddy crossing time. At the end of the period, a new location for the particle is calculated. Further discussion about the stochastic dispersion of particles can be found in Shuen et al. [45].

2.5 Fluid flow equations

Since the presence of particles influences the governing equations for fluid flow, a few assumptions are made in this section to provide proper forms of equations.

1. Continuity equation remains the same as a single phase.

2. Particles diffusion should be presented in energy equation due to considerable impacts on heat transfer.

3. Brownian, thermophoretic and turbulent diffusions are considered as mass diffusion terms on the right-hand side of energy equation.

With the above-mentioned assumptions, the governing equations are:

$$\frac{\partial \overline{u}_i}{\partial x_i} = 0 \tag{24}$$

$$\rho_m u_j \frac{\partial \overline{u}_i}{\partial x_j} = -\frac{\partial \overline{P}}{\partial x_i} + \frac{\partial}{\partial x_j}\left[\mu_m \frac{\partial \overline{u}_i}{\partial x_j} - \rho \overline{u_i' u_j'}\right] + g_i \rho_m \tag{25}$$

$$\rho_m \overline{u}_j \frac{\partial \overline{T}}{\partial x_j} = \frac{1}{c_{P_m}} \frac{\partial}{\partial x_j} \left[k_m \frac{\partial \overline{T}}{\partial x_j} - \rho_m c_{P_m} \overline{T' u'_j} \right] + \rho_p \left[(D_b + \varepsilon_t) \frac{\partial C}{\partial x_i} \frac{\partial \overline{T}}{\partial x_i} + \frac{D_T}{\overline{T}} \frac{\partial \overline{T}}{\partial x_i} \frac{\partial \overline{T}}{\partial x_i} \right] \tag{26}$$

$$D_T = 0.26 \frac{k_c}{k_p + 2k_c} C \frac{\mu_c}{\rho_c} \tag{27}$$

$$D_b = \frac{K_B T}{3\pi \mu_c d_p} \tag{28}$$

where D_b, ε_t and D_T are particle diffusion coefficients for concentration, turbulence and thermophoresis, respectively. C is the particles concentration. The transport equations for the turbulent kinetic energy (κ), dissipation rate (ε) and viscosity based on $\kappa - \varepsilon$ Realizable model are as follows [46] :

$$\frac{\partial}{\partial x_i}(\rho \kappa u_i) = \frac{\partial}{\partial x_i} \left(\left[\mu + \frac{\mu_t}{\sigma_k} \right] \frac{\partial \kappa}{\partial x_i} \right) + G_k + G_b - \rho \varepsilon - Y_M + S_k \tag{29}$$

$$\frac{\partial}{\partial x_i}(\rho \varepsilon u_i) = \frac{\partial}{\partial x_i} \left(\left[\mu + \frac{\mu_t}{\sigma_\varepsilon} \right] \frac{\partial \varepsilon}{\partial x_i} \right) + \rho C_1 S \varepsilon - \rho C_2 \frac{\varepsilon^2}{\kappa + \sqrt{\nu \varepsilon}} + C_{1\varepsilon} \frac{\varepsilon}{\kappa} C_{3\varepsilon} G_b + S_\varepsilon \tag{30}$$

$$\mu_t = \rho C_\mu \frac{\kappa^2}{\varepsilon} \tag{31}$$

$$C_1 = max \left[0.43, \frac{S \frac{\kappa}{\varepsilon}}{S \frac{\kappa}{\varepsilon} + 5} \right] \tag{32}$$

$$C_2 = 1.9, \sigma_k = 1.0, \sigma_\varepsilon = 1.2, C_{1\varepsilon} = 1.44 \tag{33}$$

$$C_\mu = \frac{1}{A_0 + A_s \frac{\kappa U^*}{\varepsilon}}, \tag{34}$$

where S and $C_{3\varepsilon}$ are the rate of strain tensor and degree to which ε is influenced by the buoyancy, respectively. A_0, U^* and A_s are functions of the mean rate of strain tensor.

Turbulent diffusivity plays the most significant role in heat transfer. Three methods are suggested to calculate particle turbulent diffusion as:

1. Since the transport mechanism is the same in mass, momentum, and energy, the particle turbulent diffusivity can be estimated as eddy diffusivity or turbulent thermal diffusivity [47].

$$\varepsilon_t = \frac{\mu_t}{Sc_t} \tag{35}$$

where μ_t and Sc_t are turbulent viscosity and Schmidt number. Turbulent Schmidt number can be assumed between 0.7 to 1 [47].

2. The order of turbulent diffusivity is similar to the first approach in second method as follows[33]:

$$\varepsilon_t = \mu_t \left(1 + 0.85 \frac{\left| u_c - u_p \right|^2}{2\kappa / 3} \right)^{-0.5} \tag{36}$$

3. In the third method, more particle parameters are involved in the calculation of turbulent diffusivity [46]. The user defined function of this method is implemented in the energy equation.

$$\varepsilon_t = C_\mu \frac{\kappa^2}{\varepsilon} \left(\frac{\gamma}{1+\gamma} \right) \left(1 + C_\beta \lambda^2 \right)^{-0.5} \tag{37}$$

$$\lambda = \frac{\left| u_p - u_c \right|}{\sqrt{2/3\kappa}} \tag{38}$$

$$C_\beta = 1.8 - 1.35 \cos^2 \theta \tag{39}$$

$$\cos\theta = \frac{\left(u_p - u_c\right).u_p}{\left|u_p - u_c\right|\left|u_p\right|} \tag{40}$$

where γ is the time ratio between the affected time scale of the turbulent eddies (τ_s) and the particle relaxation time (τ_p). C_μ is assumed constant here and equal to 0.09.

$$\gamma = \frac{\tau_s}{\tau_p} \tag{41}$$

$$\tau_p = \frac{\rho_p d_p}{18\mu_c} \tag{42}$$

$$\tau_s = \frac{\tau_0}{\sqrt{1 + C_\beta \lambda^2}} \tag{43}$$

$$\tau_0 = 3C_\mu \frac{\kappa}{2\varepsilon} \tag{44}$$

The reasons that the third method was chosen are as follows. Firstly, the values for the first and second methods are at the same order. Secondly, the effect of nanoparticles on the particle turbulent diffusion is pronounced in the third method, by considering the impacts of relative velocity, particles diameter and particle relaxation time.

Each part of the proposed method was used in various types of flow, from particles in any scale to bubbly flows, in different occasions. For instance, a combination of discrete model, Eulerian two-phase model and turbulent diffusivity can be found in literature[48–50]. Although, only some interactions with conventional heat transfer model were employed.

2.6 Mixture properties

The mixture properties of alumina and zirconia nanofluids are presented here [32]:

$$\rho_m = \sum_{k=1}^{2} C_k \rho_k \tag{45}$$

$$C_{P_m} = \frac{\sum_{k=1}^{2} C_k \rho_k C_{P_k}}{\rho_m} \tag{46}$$

The transport properties for alumina:

$$\frac{k_m}{k_c} = 1 + 4.5503C \tag{47}$$

$$\frac{\mu_m}{\mu_c} = exp\left(4.91C \Big/ (0.2092 - C)\right) \tag{48}$$

The transport properties for zirconia:

$$\frac{k_m}{k_c} = 1 + 2.4505C - 29.867C^2 \tag{49}$$

$$\frac{\mu_m}{\mu_c} = exp\left(11.19C \Big/ (0.196 - C)\right) \tag{50}$$

3. Numerical considerations

ANSYS Fluent 17.0 was employed to simulate particle-fluid flow in this study. Second order scheme was chosen for energy, momentum, turbulent kinetic energy and turbulent dissipation rate and also PRESTO! for pressure interpolation. The best criterion for the final solution was found to be the balance of heat transfer when it was in less than 2% error.

The realizable two-equation model was used with scalable wall function as the wall treatment model. The other schemes and wall treatment were also examined, but they failed to be in good agreement with the experiments. Also, the convergence was found faster with the suggested schemes and the wall treatment.

3.1 Numerical procedure

Due to many modifications in the basic equations, the method of simulation is extensively explained here.

1. At the first step, the flow and energy equations are solved for base fluid in the turbulent regime.

2. When the solution is converged, the Brownian force and particle heat transfer equation are implemented as user-defined functions (UDFs), and discrete phase is solved for one iteration.

3. After particles calculation, the particles turbulent diffusivity is calculated and stored in a memory function.

4. Then, a UDF for a new scalar field is executed and particles concentration distribution is stored in it.

5. An adjust function for temperature is executed to calculate the gradient of temperature.

6. All the fluid properties are changed and implemented based on the new concentration scalar.

7. The source terms for energy equation are implemented as another UDF.

8. The simulation goes on to reach a final acceptable solution.

4. Results and discussion

The simulation results of alumina and zirconia nanofluids in the turbulent flow are presented in this section and compared to experimental measurements. The validations were conducted for both of heat transfer and friction coefficient.

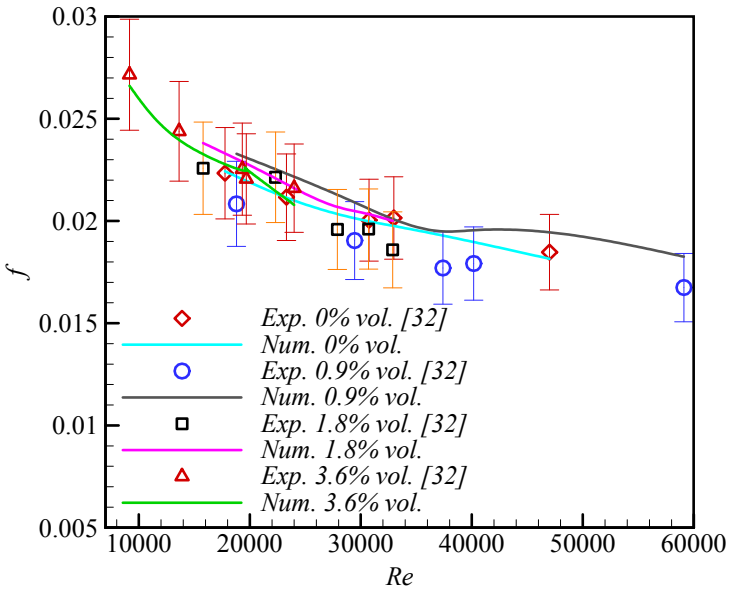

a)

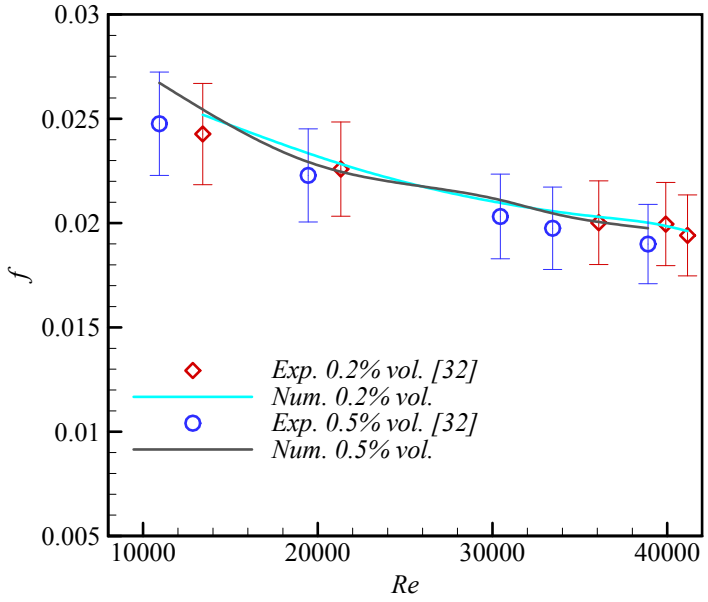

b)

Figure 1. Friction coefficient for a) alumina and b) zirconia nanofluid in turbulent flow

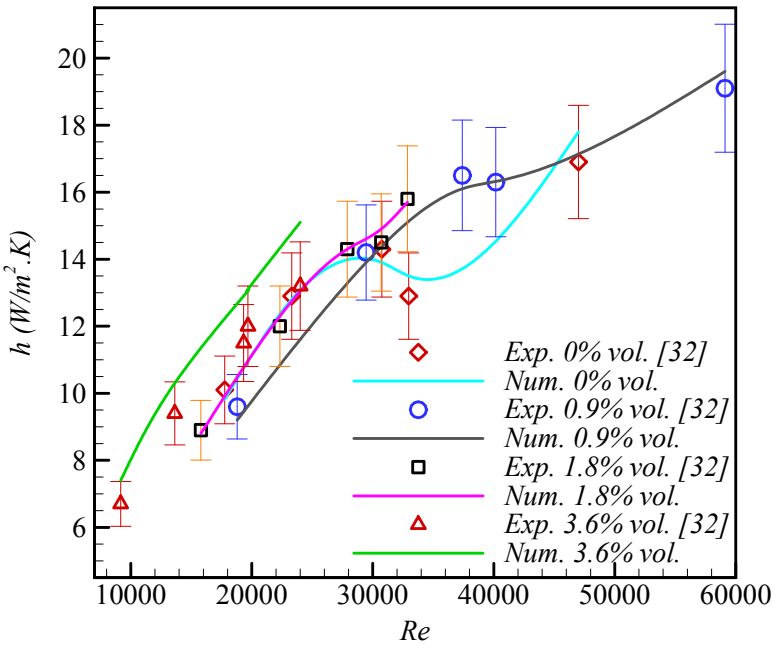

a)

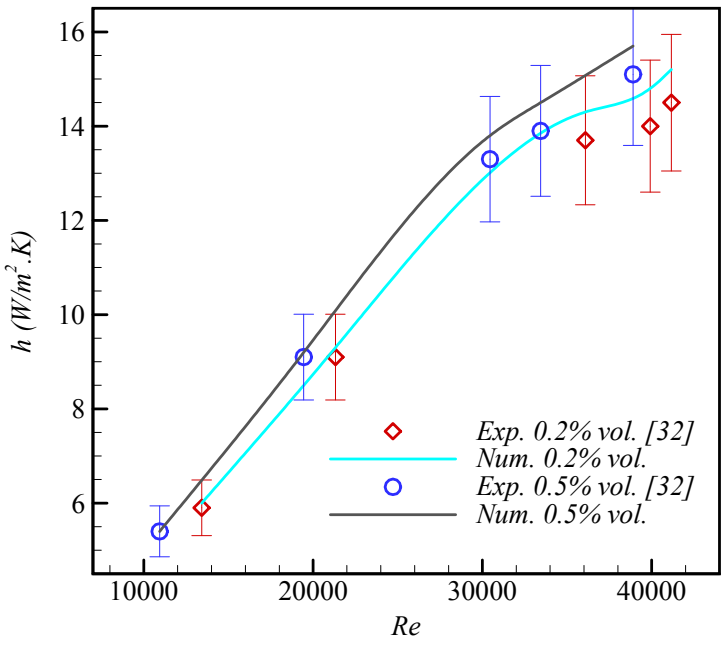

b)

Figure 2. Heat transfer coefficient for a) alumina and b) zirconia nanofluid in turbulent flow

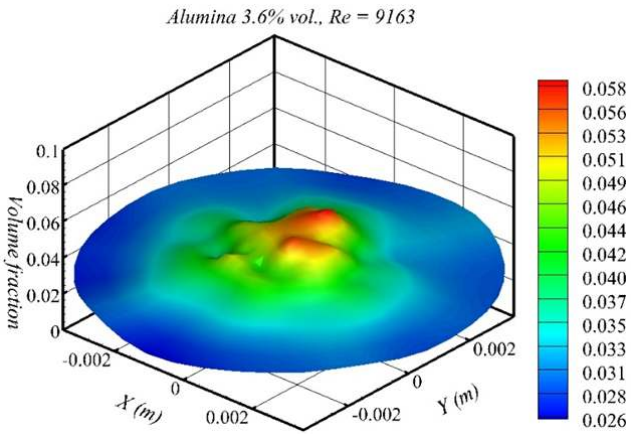

a)

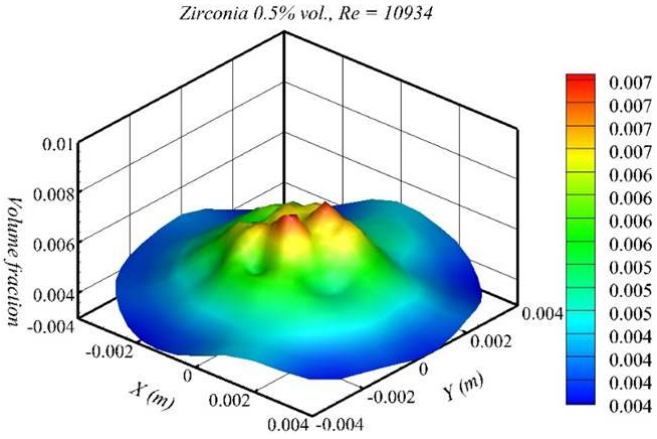

f)

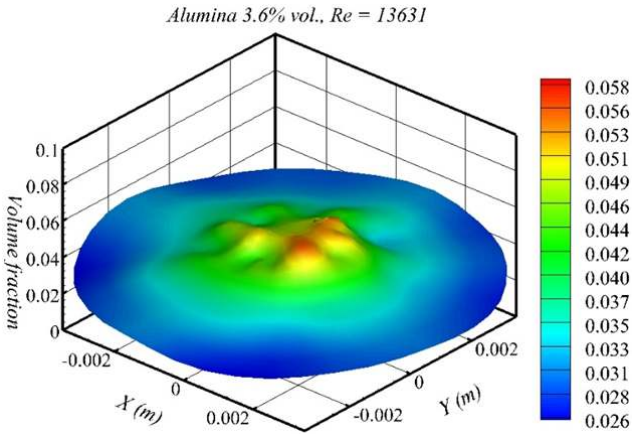
Alumina 3.6% vol., Re = 13631
Volume fraction
X (m)
Y (m)

b)

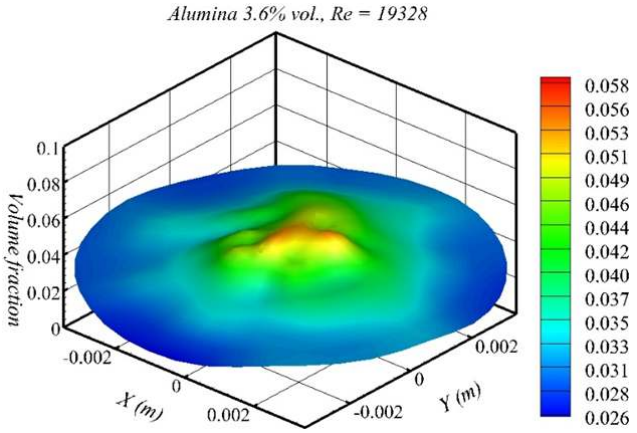
Alumina 3.6% vol., Re = 19328
Volume fraction
X (m)
Y (m)

c)

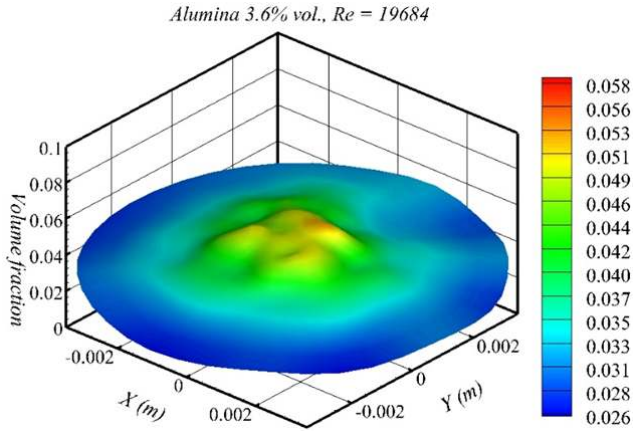
Alumina 3.6% vol., Re = 19684
Volume fraction
X (m)
Y (m)

d)

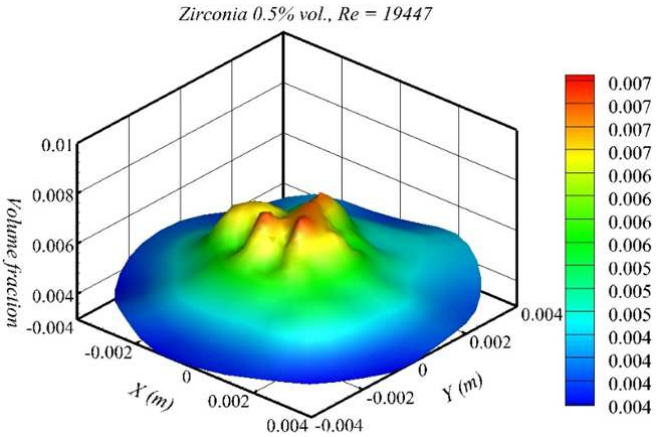
Zirconia 0.5% vol., Re = 19447
Volume fraction
X (m)
Y (m)

g)

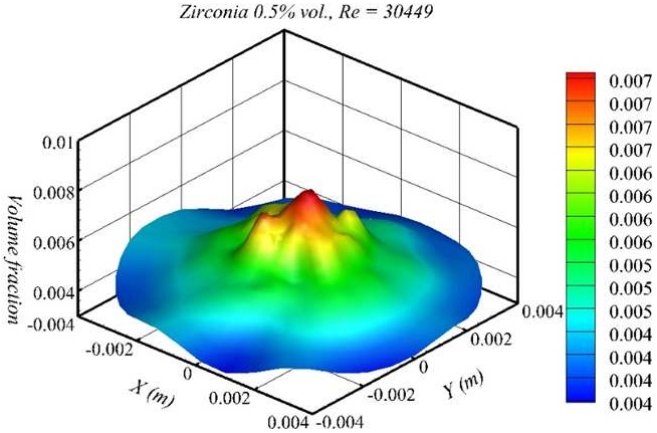
Zirconia 0.5% vol., Re = 30449
Volume fraction
X (m)
Y (m)

h)

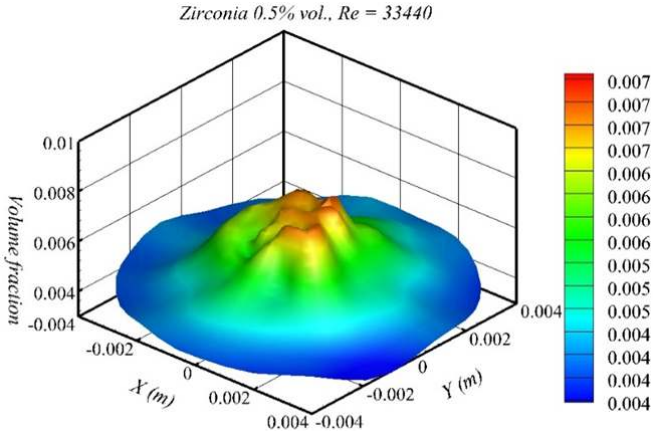
Zirconia 0.5% vol., Re = 33440
Volume fraction
X (m)
Y (m)

i)

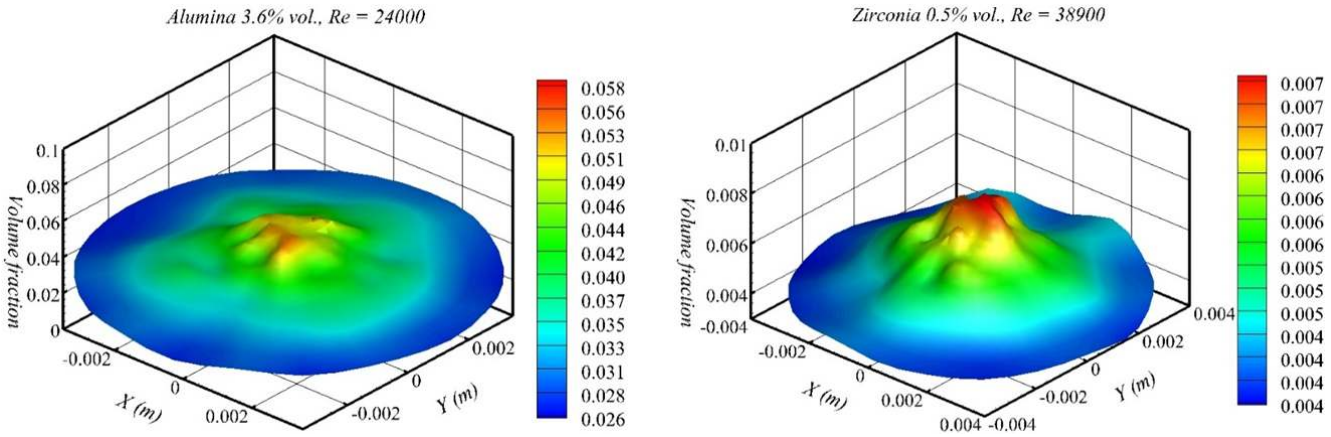

e) j)

Figure 3. Volume fraction distribution of particles at the outlet of the horizontal tube for alumina and zirconia.

The simulations results for friction coefficient and heat transfer coefficient in turbulent horizontal tube flow are compared to experimental measurements in figure 1 and 2. The error bars are ±10% of the measured values[51]. The details about Reynolds number, inlet velocity, tube diameter and particle type/loading are available in Table 1. The results are less than 10% error for most of the cases and in good agreement with experiments. Therefore, the accuracy of the proposed method is confirmed.

The advantages of the new method in this report are mainly concerned with the details of changes in fluid flow and particles migration which are predicted and presented in this section.

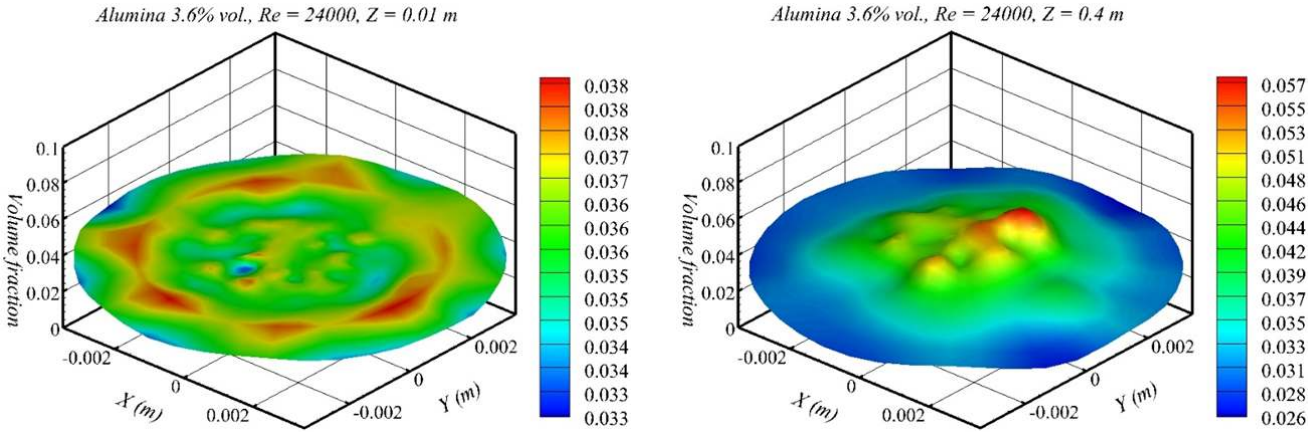

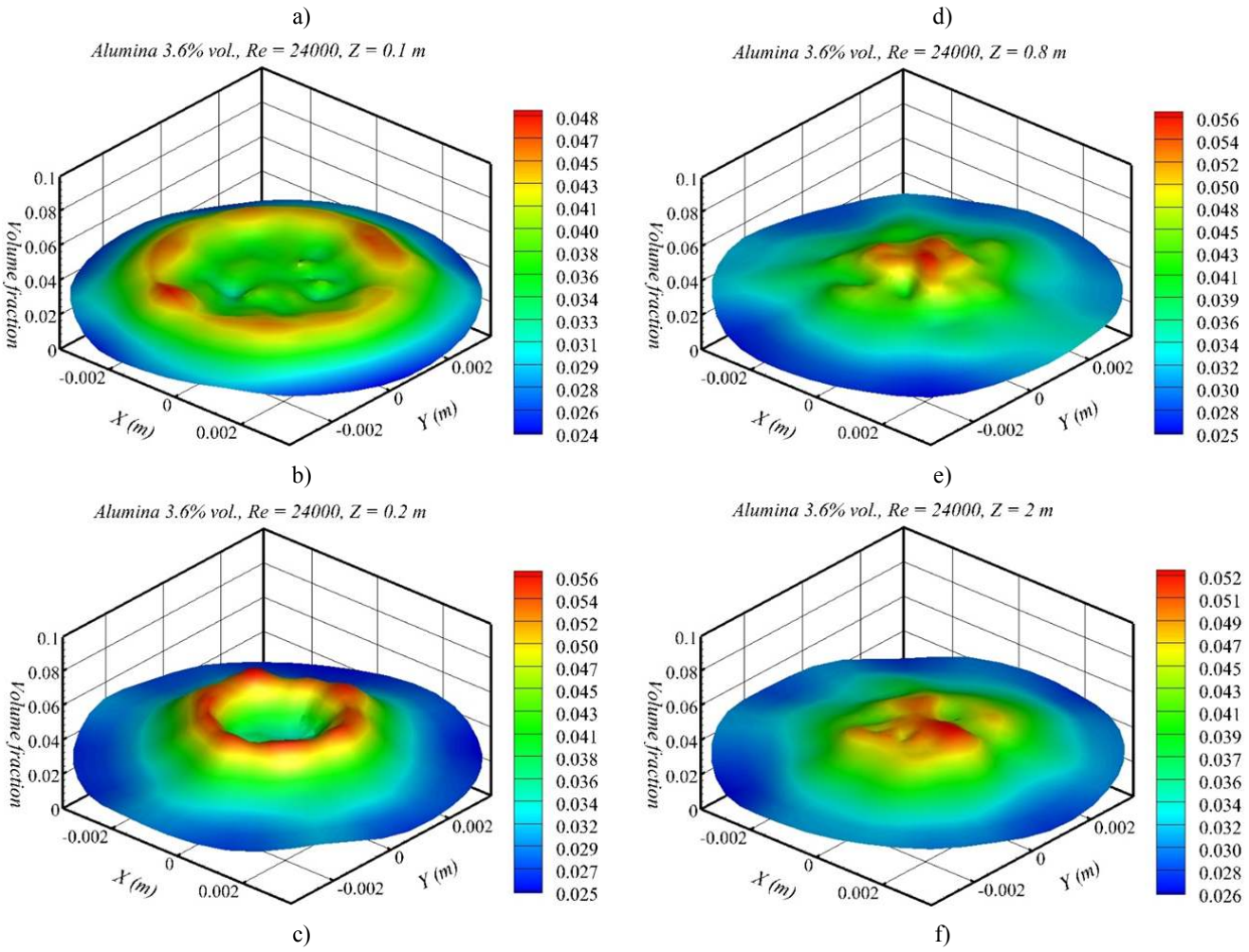

Figure 4. Particle migrations toward the centre of the horizontal tube from the inlet to the outlet at different cross sections for alumina nanofluid 3.6vol%.

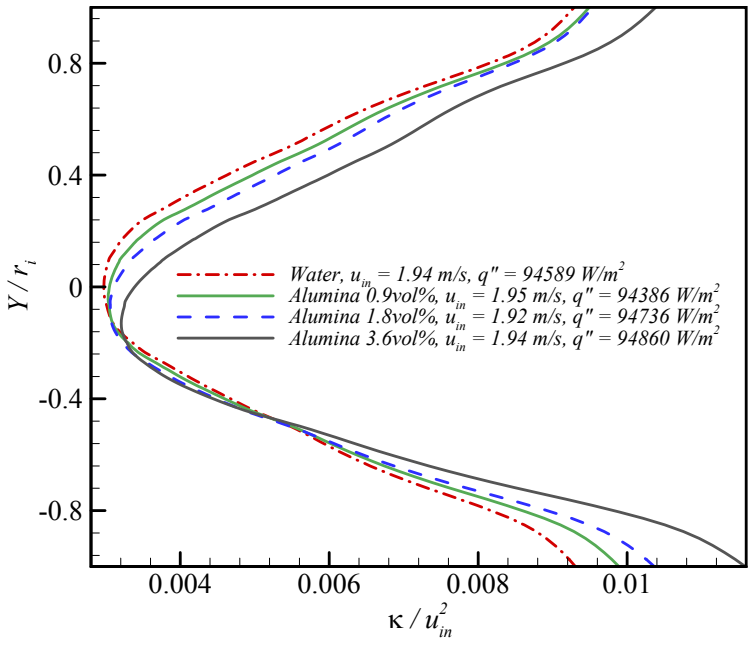

a)

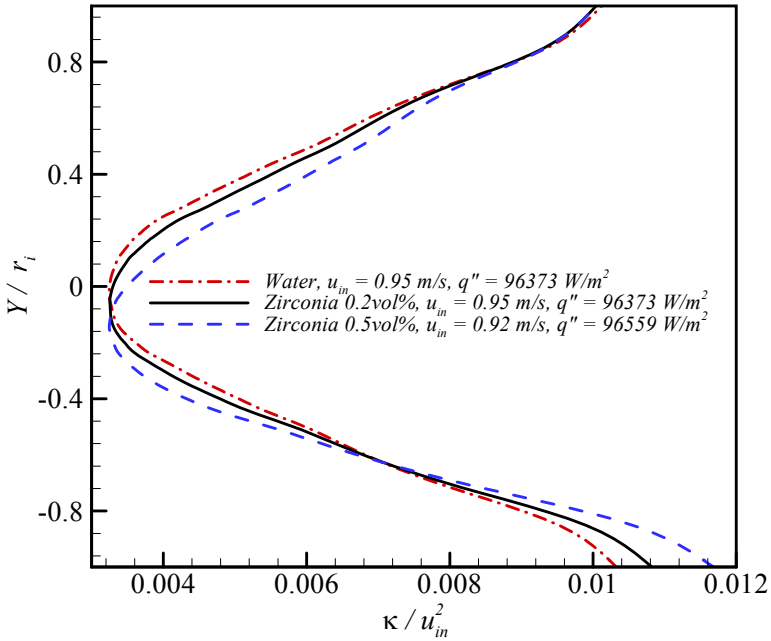

b)

Figure 5. Development of fluid turbulent kinetic energy at the outlet of the horizontal tube for a) alumina and b) zirconia nanofluid.

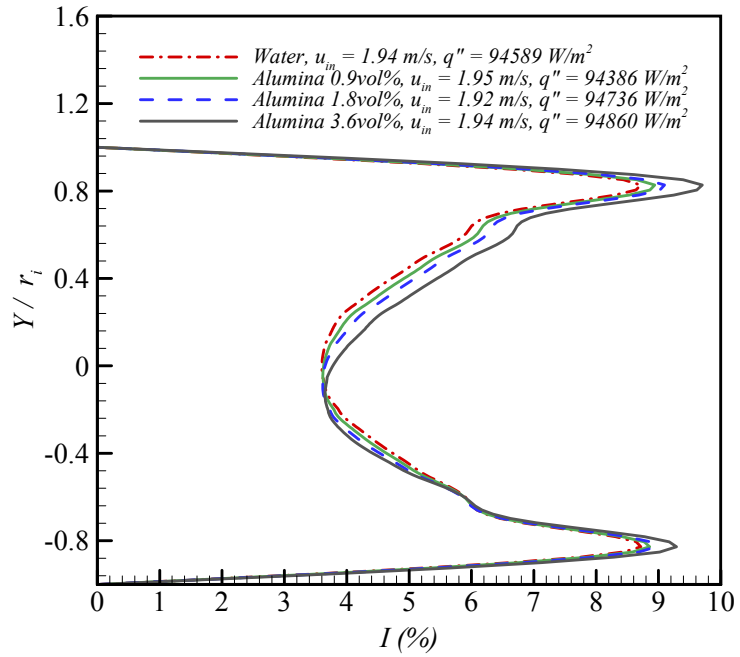

a)

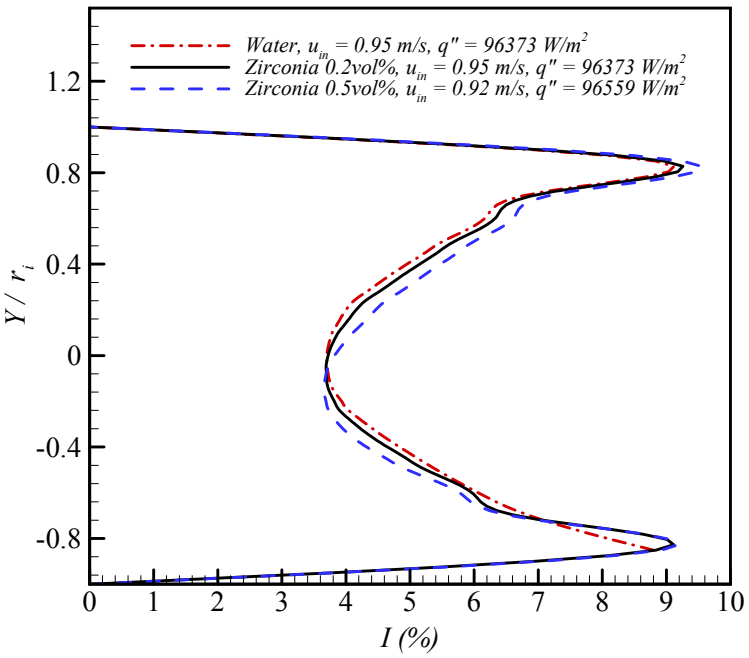

b)

Figure 6. Development of turbulent intensity for different volume fraction a) alumina and b) zirconia nanofluids.

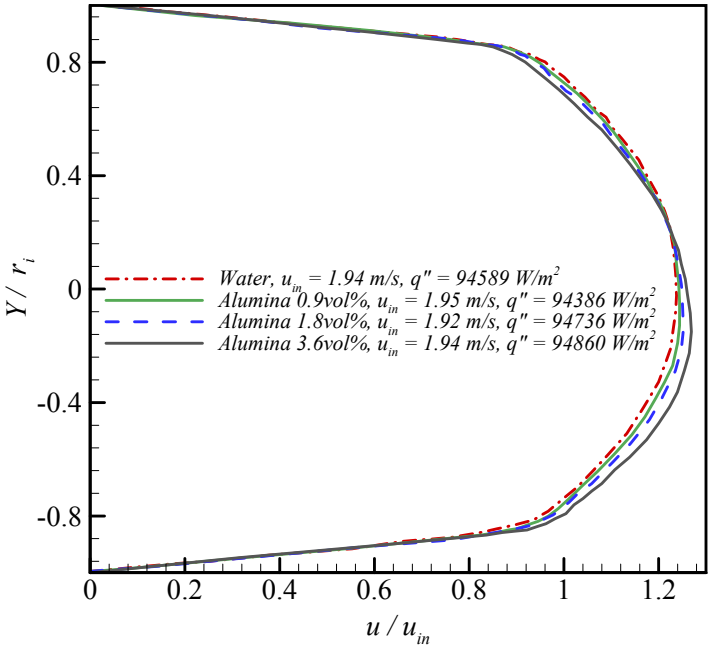

a)

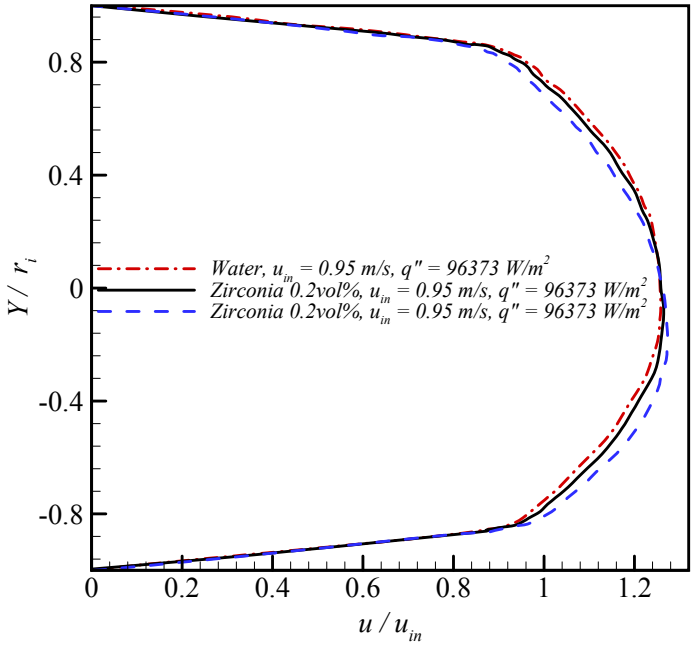

b)

Figure 7. Variations of mean fluid velocity due to the presence of particles for a) alumina and b) zirconia nanofluids.

Table 1. Details of some parameters used in the simulations

Reynolds number	u_{in}(m/s)	Tube diameter *D (m)*	Al_2O_3 volume fraction	ZrO_2 volume fraction
$\frac{\rho_m u_{in} D}{\mu_m}$, 9000 - 60000	*0.92 – 3.5*	*0.0094*	*0.9% - 3.6%*	*0.2% and 0.5%*

Variations in volume fraction distribution of alumina and zirconia nanofluids in a cross section of the horizontal tube for different Reynolds number are illustrated in figure 3. The trend in particles migration can be easily seen for both fluids. The non-uniformity of distribution is more visible at lower Reynolds number comparing to higher ones.

It can be justified because of the velocity profile intends to be flatter in higher Reynolds number, so the particles are uniformly distributed throughout the flow. Also, the concentrated area always remains to be around the centre of the tube in turbulent flow. The other turbulent parameters can provide a better explanation for these phenomena.

Evolution of particles volume fraction from the inlet to the outlet at different cross sections is illustrated in figure 4. The distribution is almost uniform at the beginning. Then, particles migrate toward the centre of the flow due to strong effects of fluctuating velocity and eddies with higher kinetic energy close to the wall, shown in figure 5. Therefore, particles are influenced by higher kinetic energy region to move to lower kinetic energy regions. These results prove the significance of considering both distributions of particles due to fluctuating velocity and turbulent diffusion source term added to the energy equation.

Turbulent intensity is defined as the root mean square of turbulent velocity fluctuation over local mean velocity. The presence of particles in the fluid increases turbulent kinetic energy and intensity, shown in figure 5 and figure 6. The trend is similar for both alumina and zirconia nanofluid. Turbulence intensity also rises with an increase in particles concentration. Growth in

turbulent kinetic energy and intensity is the main reason for an increase in pressure loss with adding particles to the fluid. On the other hand, nine percent intensity is clearly enough to drag the particles from close to the wall to the central region of the flow with intensity less than 5%.

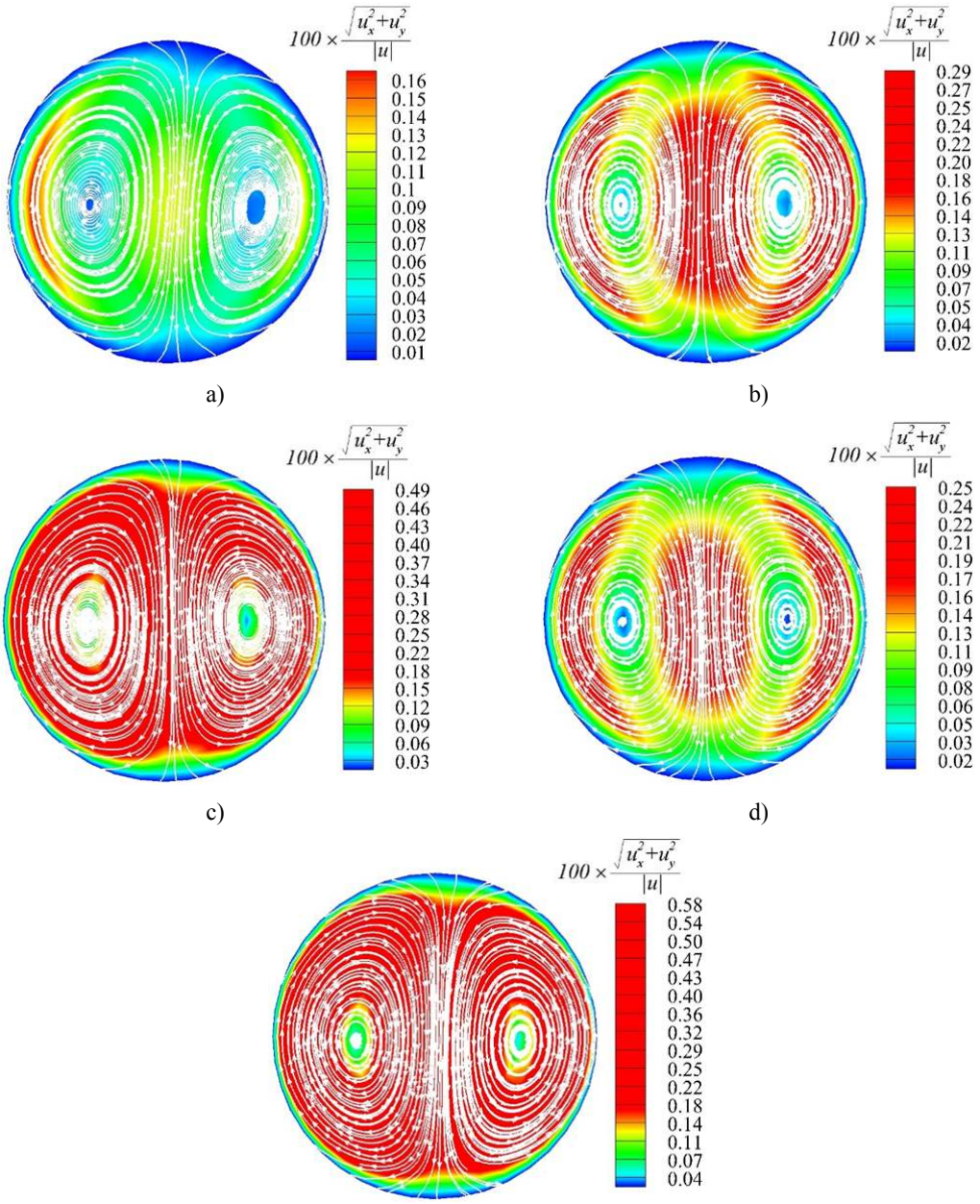

Figure 8. Contours of strength and streamtrace of secondary flow induced by particles for a) alumina 0.9% vol. b) alumina 1.8% vol. c) alumina 3.6% vol. d) zirconia 0.2% vol. and e) zirconia 0.5% vol.

The impacts of particles on flow mean velocity is presented in figure 7. It is observed that there is always a location where the flow mean velocity is not affected by the particles, which is not clear at the centre of the horizontal tube. It can be explained as follows: Brownian force and the influences of fluctuating velocity are the only forces acting in all directions, while other important forces such as thermophoresis, lift and Magnus only act toward the centre of the tube. On the other hand, Brownian diffusion can be only important close to the wall and not in the main flow comparing to turbulent diffusion.

It means that only some of the forces can cancel each other at the centre of the tube and the influences of random fluctuation velocity remain strong in the main flow. This can somehow change the position where the maximum mean velocity used to occur, meaning the centre of the tube.

In the other word, the particles distort the flow velocity profile and move the position of maximum mean velocity from the centre to lower position. This phenomenon can be easily captured at higher concentration of alumina nanofluid 3.6% vol. This was also reported by Laín and Sommerfeld [52], except they explained bouncing off the particles from the wall toward the centre as the contributing factor, rather than the impacts of fluctuation. While turbulent diffusion and fluctuating velocity play a significant role in this study due to nanoscale size of the particles.

Table 2. Strength of secondary flow induced by particles

	Alumina 0.9%vol.	Alumina 1.8%vol.	Alumina 3.6%vol.	Zirconia 0.2%vol.	Zirconia 0.5%vol.
Strength of secondary flow	0.09%	0.18%	0.31%	0.16%	0.36%

The other interesting aspect of the proposed model in this study is reported in figure 8 and table 2. A secondary flow at the cross section of the tube is induced due to impacts of particles on the flow. A strength secondary flow parameter is defined as the magnitude of secondary flow over total velocity magnitude as

$\sqrt{u_x^2 + u_y^2} \Big/ |u|$. As can be seen, the strength increases with a rise in particle volume fraction and also depending on the type of particles. It means that the gravity plays an important role when the density ratio reaches to almost 6 for zirconia nanoparticles.

Radial displacement of particles released from different radial locations is shown in figure 9. The random nature of particles displacement in this figure can be easily referred to fluctuation velocity. The migration covers the entire region of the flow from the centre to the vicinity of the wall. Therefore, it can be concluded that particle turbulent diffusion is the dominant phenomenon in turbulent flow.

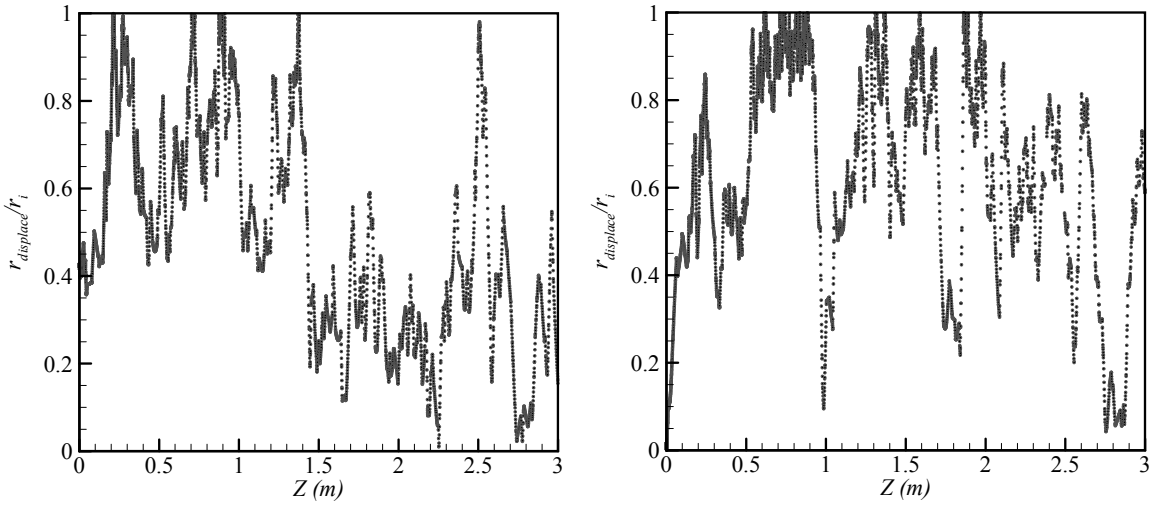

a) b)

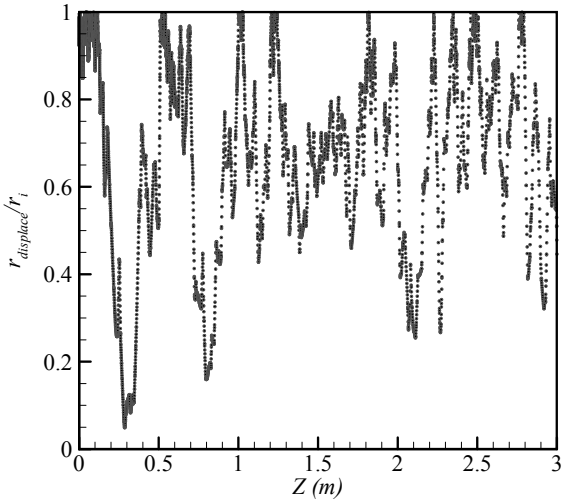

c)

Figure 9. Radial migration of particles released from different locations at the inlet for alumina nanofluid 3.6% vol.

5. Conclusion remarks

A new method is developed to simulate turbulent forced convective flow for nanofluids. Even though, it can be also used in other types of particle-liquid flows. A Brownian force and energy equation for particles are implemented as a part of solving discrete phase model. Then, the results of particles tracking are saved and imported as mixture properties in the flow equations. Due to the importance of diffusion in the case of nanoparticles, the diffusion source terms for thermophoresis, concentration and turbulence are implemented in the energy equation. At the first step, the good agreement was found between the results of the proposed model and experiment for both of heat transfer and friction coefficient for two different types of nanofluids. The advantages of this new method can be as follows: accuracy in calculation of heat transfer coefficient and pressure drop within less than 10% error, reporting concentration distribution and particles migration toward the centre of the tube, considering most of the phenomena involved in particles migration and diffusion, tracking of the particles anywhere in the flow. Also, the secondary flow induced by the impacts of the particles was properly captured in the simulations. Particles

loading showed increasing effects on the secondary flow strength, depending on the density and type of the particles. It is noted that particles cluster formation is one the important phenomenon which is needed to be considered in future studies.

Nomenclature

A_p	Particle projected area, m^2
C	Concentration
C_c	Cunningham correction factor
C_D	Drag coefficient
C_{ML}	Rotational coefficient
C_ω	Rotational drag coefficient
C_p	Specific heat, J/kg.K
d_p	Particle diameter, m
D	Tube diameter, m
D_T	Thermophoresis diffusion coefficient, m^2/s
D_b	Concentration diffusion coefficient, m^2/s
f	Friction factor
F	Drag force, N
F_b	Brownian force, N
h	Heat transfer coefficient, $W/m^2.K$
I	Turbulent intensity
I_p	Moment of inertia, kg/m^2
k	Thermal conductivity [W/m.K]
K_B	Boltzmann constant, $m^2.kg/^oK.s^2$
m_p	Particle mass, kg

r_i	Tube radius, m
$r_{displace}$	Radial displacement, m
Re	Reynolds number
Re_{ω_p}	Angular Reynolds number
Sc_t	Schmidt number
Δt_p	Particle time step, s
u	Velocity, m/s
u_i'	Fluctuating velocity, m/s
X, Y	Tube cross section, m
Z	Flow direction, m
Greek symbols	
ε	Turbulent dissipation rate, m^2/s^3
ε_t	Particle diffusion coefficient, m^2/s
$\dot{\gamma}$	Shear rate, 1/s
κ	Turbulent kinetic energy, m^2/s^2
μ	Viscosity, Pa.s
μ_t	Turbulent viscosity, Pa.s
ω_p	Particle angular velocity, 1/s
Ω	Relative particle-liquid angular velocity, 1/s
ρ	Density, kg/m^3
τ	Particle relaxation time, s
ζ_i	Gaussian white noise random number
ξ	Random number
Subscript	
c	continues phase
in	inlet

m	mixture
p	particle

Reference

[1] E. Ebrahimnia-Bajestan, M. Charjouei Moghadam, H. Niazmand, W. Daungthongsuk, and S. Wongwises, Int. J. Heat Mass Transf. **92**, 1041 (2016).

[2] I.M. Shahrul, I.M. Mahbubul, R. Saidur, and M.F.M. Sabri, Int. J. Heat Mass Transf. **97**, 547 (2016).

[3] S.S. Sonawane, R.S. Khedkar, and K.L. Wasewar, Int. Commun. Heat Mass Transf. **49**, 60 (2013).

[4] L.S. Sundar and K. V. Sharma, Int. J. Heat Mass Transf. **53**, 1409 (2010).

[5] R. Ni, S.Q. Zhou, and K.Q. Xia, Phys. Fluids **23**, (2011).

[6] B. Kolade, K.E. Goodson, and J.K. Eaton, J. Heat Transfer **131**, 52402 (2009).

[7] A.T. Utomo, E.B. Haghighi, A.I.T. Zavareh, M. Ghanbarpourgeravi, H. Poth, R. Khodabandeh, B. Palm, and A.W. Pacek, Int. J. Heat Mass Transf. **69**, 77 (2014).

[8] Y. Yang, Z.G. Zhang, E.A. Grulke, W.B. Anderson, and G. Wu, Int. J. Heat Mass Transf. **48**, 1107 (2005).

[9] K.B. Anoop, T. Sundararajan, and S.K. Das, Int. J. Heat Mass Transf. **52**, 2189 (2009).

[10] Y. He, Y. Jin, H. Chen, Y. Ding, D. Cang, and H. Lu, Int. J. Heat Mass Transf. **50**, 2272 (2007).

[11] C.. Tang, S. Tiwari, and M.W. Cox, J. Nanotechnol. Eng. Med. **4**, 21004 (2013).

[12] B. Sahin, G.G. Gültekin, E. Manay, and S. Karagoz, Exp. Therm. Fluid Sci. **50**, 21 (2013).

[13] S. Torii, Y. Satou, and Y. Koito, Int. J. Green Energy **7**, 289 (2010).

[14] Y. Xuan and Q. Li, J. Heat Transfer **125**, 151 (2003).

[15] R. Chein and J. Chuang, Int. J. Therm. Sci. **46**, 57 (2007).

[16] H. Zhang, S. Shao, H. Xu, and C. Tian, Appl. Therm. Eng. **61**, 86 (2013).

[17] D. Liu and L. Yu, J. Heat Transfer **133**, 31009 (2011).

[18] R. Ahmad, Phys. Fluids **28**, 72002 (2016).

[19] A.A. Avramenko, D.G. Blinov, and I. V Shevchuk, Phys. Fluids **23**, 82002 (2011).

[20] E.B. Öğüt and K. Kahveci, J. Mol. Liq. **224**, 338 (2016).

[21] H. Safikhan and A. Abbassi, Int. J. Therm. Sci. **109**, 114 (2016).

[22] R.D. Selvakumar and S. Dhinakaran, Int. J. Heat Mass Transf. (2016).

[23] J. Buongiorno, J. Heat Transfer **128**, 240 (2006).

[24] A.A. Avramenko, D.G. Blinov, I. V Shevchuk, and A. V Kuznetsov, Phys. Fluids **24**, 92003 (2012).

[25] M. Mahdavi, M. Sharifpur, and J.P. Meyer, Powder Technol. **307**, 153 (2017).

[26] M. Mahdavi, M. Sharifpur, H. Ghodsinezhad, and J.P. Meyer, Int. J. Heat Mass Transf. **In press**, (2016).

[27] N. Kumar and B.P. Puranik, Appl. Therm. Eng. In press (2016).

[28] M. Mahdavi, M. Sharifpur, and J.P. Meyer, Int. J. Therm. Sci. **110**, 36 (2016).

[29] M. Mahdavi, M. Sharifpur, and J.P. Meyer, Int. J. Heat Mass Transf. **88**, 803

(2015).

[30] S. Rashidi, M. Bovand, J.A. Esfahani, and G. Ahmadi, Appl. Therm. Eng. **100**, 39 (2016).

[31] K.M. Shirvan, M. Mamourian, S. Mirzakhanlari, H.F. Öztop, and N. Abu-Hamdeh, Adv. Powder Technol. **27**, (2016).

[32] W. Williams, J. Buongiorno, and L.-W. Hu, J. Heat Transfer **130**, 42412 (2008).

[33] M. Manninen, V. Taivassalo, and S. Kallio, *On the Mixture Model for Multiphase Flow* (Technical Research Centre of Finland Finland, VTT publications 288, 1996).

[34] X. Zheng and Z. Silber-Li, Appl. Phys. Lett. **95**, 24 (2009).

[35] P.G.T. Saffman, J. Fluid Mech. **22**, 385 (1965).

[36] W. Kraipech, A. Nowakowski, T. Dyakowski, and A. Suksangpanomrung, Chem. Eng. J. **111**, 189 (2005).

[37] B. Oesterle and T.B. Dinh, Exp. Fluids **25**, 16 (1998).

[38] S.C.R. Dennis, S.N. Singh, and S.B. Ingham, J. Fluid Mech. **101**, 257 (1980).

[39] G.S. McNab and A. Meisen, J. Colloid Interface Sci. **44**, 339 (1973).

[40] A. Li and G. Ahmadi, Aerosol Sci. Technol. **16**, 209 (1992).

[41] O. Abouali, A. Nikbakht, G. Ahmadi, and S. Saadabadi, Aerosol Sci. Technol. **43**, 205 (2009).

[42] G.E.P. Box, M.E. Muller, and others, Ann. Math. Stat. **29**, 610 (1958).

[43] E.E. Michaelides and Z. Feng, Int. J. Heat Mass Transf. **37**, 2069 (1994).

[44] M. Bayazit, J. Hydraul. Res. **10**, 1 (1972).

[45] J.-S. Shuen, L.-D. Chen, and G.M. Faeth, AIChE J. **29**, 167 (1983).

[46] Ansys-Fluent, Canonsburg, PA, USA ANSYS Inc (2016).

[47] D. Eskin, J. Ratulowski, K. Akbarzadeh, and T. Lindvig, WIT Trans. Eng. Sci. **63**, 85 (2009).

[48] M.A. Pakhomov and V.I. Terekhov, Int. J. Heat Mass Transf. **92**, 689 (2016).

[49] H.A. Mrabtini, G. Bellakhal, and J. Chahed, Nucl. Eng. Des. J. **320**, 112 (2017).

[50] E. Alméras, C. Plais, F. Euzenat, F. Risso, V. Roig, and F. Augier, Chem. Eng. Sci. **140**, 114 (2016).

[51] W.C. Williams, Experimental and Theoretical Investigation of Transport Phenomena in Nanoparticle Colloids (Nanofluids), Massachusetts Institute of Technology, 2007.

[52] S. Laín and M. Sommerfeld, Int. J. Multiph. Flow **39**, 105 (2012).